Available online at www.sciencedirect.com

ScienceDirect

Ceramics International 40 (2014) 5097–5102

CERAMICS INTERNATIONAL

www.elsevier.com/locate/ceramint

Short communication

Microstructure and the dielectric properties of SiCN–Si_3N_4 ceramics fabricated via LPCVD/CVI

Xiaofei Liu, Litong Zhang, Yongsheng Liu*, Fang Ye, Xiaowei Yin

Science and Technology on Thermostructure Composite Materials Laboratory, Northwestern Polytechnical University, Xi'an, Shaanxi 710072, China

Received 16 August 2013; received in revised form 28 September 2013; accepted 28 September 2013
Available online 8 October 2013

Abstract

SiCN–Si_3N_4 ceramics were fabricated by infiltrating SiCN into porous Si_3N_4 ceramics with different flux ratio of precursor gases via low-pressure chemical vapor deposition/infiltration (LPCVD/CVI). Several methods of characterization were employed to discuss the effects of different precursor gases ratio on the microstructure and dielectric properties of fabricated SiCN–Si_3N_4 ceramics. The deposition product is amorphous and mainly consists of Si–N, C–C and Si–C bonds. In SiCN–Si_3N_4 ceramics, free carbon disperses uniformly in the amorphous and low-conductivity SiCN, which results in suitable dielectric properties. The mean real part (ε') and imaginary part (ε'') of permittivity increase from 3.82 and 0.05 to 7.71 and 6.94, respectively. The dielectric loss (tan δ) can be controlled from 0.014 to 0.899 by changing the flux ratio of C_3H_6.

Keywords: Amorphous; Chemical vapor deposition/infiltration; Dielectric materials/properties; Silicon carbonitride

1. Introduction

In recent years, materials absorbing electromagnetic wave (EMW) have attracted worldwide attention because of the urgent need to protect the workspace and environment as a result of the development of microwave-absorbing technology [1,2]. Microwave absorbing materials, being able to absorb the incident radiation, have been critically needed for lightweight, flexibility, broadband and heat stability [2]. Silicon carbonitride (SiCN) is promising for EMW absorbing application because of its attractive properties such as corrosion resistance, high temperature oxidation resistance, hardness and wide band gap, high temperature piezoresistivity, magnetic and electrical behavior [3–7]. Quan Li et al. [8] prepared SiCN–Si_3N_4 ceramic by precursor infiltration pyrolysis (PIP), which attained a mean dielectric loss of 0.202 with the largest real and imaginary permittivity of 8.9 and 1.8. Dielectric loss represents the ability to effectively convert the electromagnetic energy into heat energy which means dielectric properties of SiCN studied by Quan Li et al. need to be improved. R. Bhandavat et al. [9] found that the polymer-derived ceramic Si(B)CN-carbon nanotube composite could dissipate 72.5% of incident power as heat at 2.45 GHz where the SiCN was used as nonconducting polymer matrix and carbon nanotube was the EMW absorber. Izumi and Oda [10] found that the dielectric constant of the SiCN films by HWCVD method could be adjusted from 2.9 to 7 by changing CVD processing parameter. Although many significant and encouraging results of SiCN have been reported in previous works [9–12], till now its absorbing properties are not satisfactory and required to be improved. Simultaneously, main focus of SiCN made by CVD is the thin films, so it is necessary to develop the high performance SiCN matrix with EMW absorbing properties by low-pressure chemical vapor deposition/infiltration (LPCVD/CVI), which plays an important role in preparing for the composites [13–15]. SiCN prepared by LPCVD/CVI was amorphous and possessed low dielectric loss in previous research [16], which should be improved considerably, so the phase composition and microstructure of SiCN ceramics prepared by this method should be optimized.

*Corresponding author. Tel.: +86 29 8849 6068 807; fax: +86 29 8849 4620.
E-mail addresses: yongshengliu@nwpu.edu.cn, liuys99067@163.com (Y. Liu).

0272-8842/$ - see front matter
http://dx.doi.org/10.1016/j.ceramint.2013.09.126

Because the free carbon is an excellent microwave absorbing material and amorphous phase possesses the higher resistivity, free carbon with high conductivity dispersing uniformly in the amorphous SiCN possessing low conductivity could improve the electrical property, resulting in the improved dielectric loss. To obtain better dielectric properties, developing a carbon-rich SiCN should be a good choice.

In this study, SiCN–Si_3N_4 ceramics were fabricated by infiltrating SiCN into porous Si_3N_4 ceramics via LPCVD/CVI from the $SiCl_4$–C_3H_6–NH_3–H_2–Ar system. The effects of different precursor gases ratio on the microstructure and dielectric properties of fabricated SiCN–Si_3N_4 ceramics were discussed in detail.

2. Experimental procedures

Si_3N_4 ceramic with high porosity fabricated using the previous method [17] was machined into specimens with dimensions of $22.86 \times 10.16 \times 2.16\ mm^3$ for dielectric properties measurement and then placed into a vertical CVD/CVI furnace to infiltrate SiCN from silicon tetrachloride ($SiCl_4 \geq 99.99$ wt%), propylene ($C_3H_6 \geq 99.99\%$), ammonia ($NH_3 \geq 99.99\%$), hydrogen ($H_2 \geq 99.99\%$) and argon ($Ar \geq 99.9\%$). Hydrogen was used as the carrier gas of $SiCl_4$ and dilution gas. Argon was the dilution gas also. The sample of initial condition was named as S, when the Si/N and C/N were 1.70 and 1.80, respectively. The rest of samples were named as SS and SSC when increasing the flux of $SiCl_4$ and changing the flux of C_3H_6 based on the increased flux of $SiCl_4$. Specific processing conditions are shown in Table 1.

The morphologies of the ceramics were observed by scanning electron microscopy (SEM, S-4700; Hitachi, Japan). The elemental composition was qualitatively analyzed by EDS (Genesis XM2, EDXA, USA) attached to SEM. The phases of coatings were characterized by X-ray diffraction (XRD, D8-Advance, Bruker). X-ray photoelectron spectra (XPS) for chemical and compositional analyses were recorded on the sample surface using a Thermo scientific X-ray photoelectron spectrometer (XPS, K-Alpha; Thermo Scientific). Laser Raman micro-spectroscopy (LRMS) was taken on a Renishaw Ramoscope (Confocal Raman Microscope; inVia; Renishaw, Gloucestershire, UK) equipped with a He–Ne laser (514 nm). The relative complex permittivity (ε) of the SiCN–Si_3N_4 ceramic was measured with a network analyzer (VNA, MS4644A; Anritsu, Japan) using the waveguide method in the frequency range of 8.2–12.4 GHz according to ASTM D5568-08. ε can be expressed as

$$\varepsilon = \varepsilon' - j\varepsilon'' \quad (1)$$

where ε' is real part of the permittivity, ε'' is imaginary part of the permittivity.

3. Results and discussion

The morphologies of Si_3N_4 substrate and SiCN–Si_3N_4 ceramic are demonstrated in Fig. 1. SEM image (Fig. 1(a)) shows that porous Si_3N_4 ceramics were composed of rod-like β-Si_3N_4 intercrossing with each other. SiCN deposited via LPCVD/CVI is a cauliflower-like appearance and continuous as shown in Fig. 1(b). Also, it is well-distributed and dense, forming a crust as shown in Fig. 1(c). The morphologies of deposition product with different precursor gases ratio have no obvious difference. Fig. 1 (d) shows the energy dispersive spectroscopy (EDS) pattern of the deposition surface of SiCN–Si_3N_4 ceramics. The surface composition measured by EDS is presented in Table 2 and the data were based on the average value of five different points. This result shows that the obtained film consisted of four elements, namely Si, C, N and O. The O content was extremely low that O was probably from surface adsorption. The elemental composition changed with the deposition parameters. Elemental composition was also measured by XPS. In order to remove the surface oxygen and other attachments which caused by the adsorption from the air, Ar^+ ion sputtering was undertaken for 60 s. The XPS analysis shows that C content steadily increased from 25.7 to 62.8, while Si and N content varied from 41.1 and 33.2 to 20.4 and 16.8 accordingly. C content calculated by XPS data including adventitious hydrocarbon caused the higher C content [10], so that this elemental composition and variation tendency of elemental composition agreed well with the results of EDS except for the higher carbon content.

The typical XRD patterns of the Si_3N_4 substrate and SiCN–Si_3N_4 ceramics are shown in Fig. 2. The diffraction peaks of the SiCN–Si_3N_4 ceramics are nearly the same as that of the Si_3N_4 substrate except for the decreasing of the intensity because of the weakening of deposited product on Si_3N_4 substrate surface, which implies that the deposited SiCN is amorphous.

Raman spectroscopy-based technique is an effective method in quantitatively measuring the concentration of the free carbon [18]. The Raman spectra of SiCN–Si_3N_4 ceramics with different deposition parameters are shown in Fig. 3 The spectra of S and SS have an obvious broad amorphous peak because of the strong vibrational density of amorphous deposition and the low content of free carbon, while the spectrum of SSC has two broadening peaks. The first peak, located at 1580–1590 cm^{-1}

Table 1
Deposition conditions for SiCN–Si_3N_4 ceramic via LPCVD/CVI.

Material	T(K)	t(h)	P(Pa)	Gas flux (ml/min)			
				Si/N	C/N	H_2	Ar
S [16]	1273.15	8	2000	1.70	1.8	140	140
SS	1273.15	8	2000	4.25	1.8	140	140
SSC	1273.15	8	2000	4.25	9.0	140	140

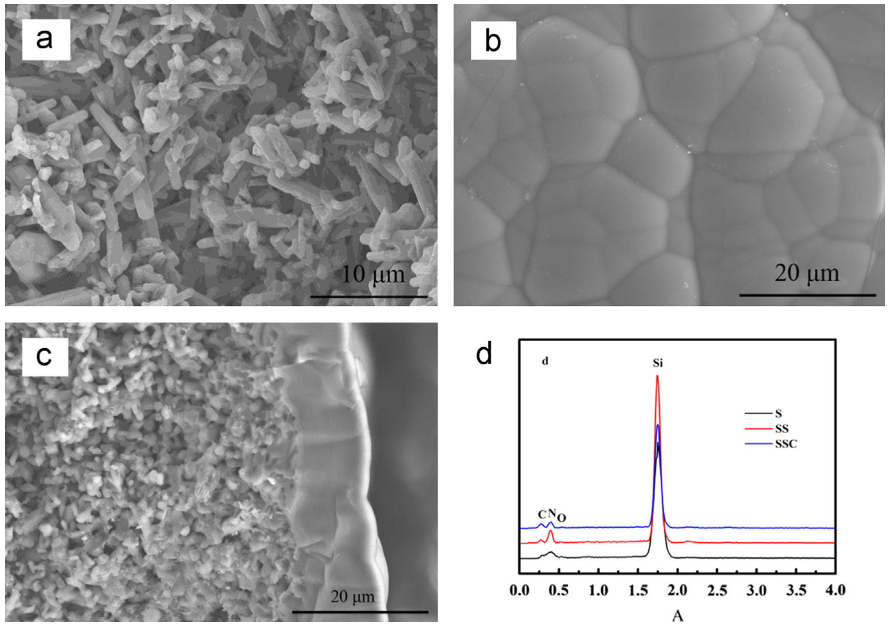

Fig. 1. Morphologies of (a) surface of Si_3N_4 substrate, (b) surface and (c) cross-section of SiCN–Si_3N_4 ceramic of SSC and (d) Energy dispersive spectroscopy pattern of the deposition surface of SiCN–Si_3N_4 ceramics.

Table 2
Elemental composition measured by EDS.

Material	Elemental composition (at%)			
	Si	N	C	O
S	38.8	39.6	19.6	2.0
SS	40.2	43.2	16.2	0.4
SSC	34.0	30.4	34.2	1.3

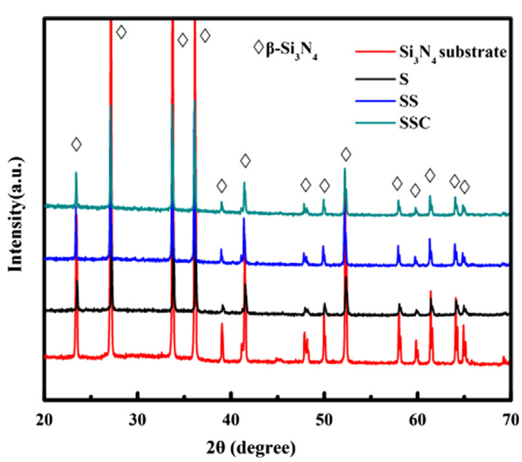

Fig. 2. XRD patterns of the Si_3N_4 substrate and SiCN–Si_3N_4 ceramics with different deposition conditions.

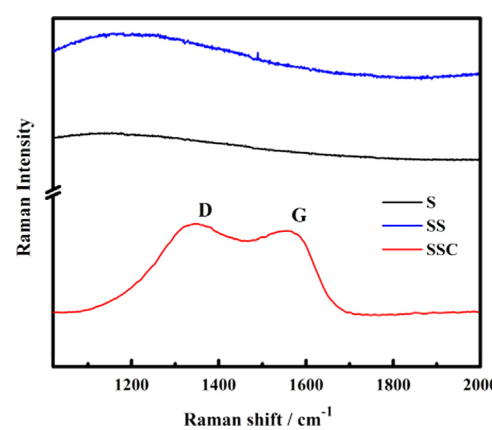

Fig. 3. Raman spectra of SiCN–Si_3N_4 ceramics with different deposition conditions.

(the G band), originates from lattice rations in the plane of the graphite-like rings. The second peak, located at around 1350 cm^{-1} (the D band), only occurs in graphite with small crystal size and increases with the amount of “unorganized” carbon in the SiCN–Si_3N_4 ceramics [19,20]. There are no additional peaks except the broadening and overlapped D and G band, which suggest the presence of a strong disorder form of the free carbon [21]. The size of the free carbon nanodomains (La) is calculated using the following equation [22]:

$$I_D/I_G = C'(\lambda)\mathrm{La}^2 \quad (2)$$

where I_D and I_G are the intensity of the D band and G band, respectively, and the $C'(\lambda)$ is about 0.0055 with $\lambda=514$ nm. The La of SSC is about 1.38 nm. Free carbon is an important component of SiCN and the flux of C_3H_6 is the key factor of the generation amount of free carbon. Consequently, SSC may be the desired material with the carbon-rich microstructure. Similar conductive structure has been confirmed in polymer-derived silicon oxycarbides [23].

The structure, nature of bonding and the composition of the nanostructural play an important role in deciding the properties of the materials. XPS was carried out to confirm the bonding structure of the amorphous SiCN. Fig. 3 shows the high-resolution XPS spectra of C1*s* levels for (a) S, (b) SS, (c) SSC and (d) Si2*p* core levels for SSC. The correction of the XPS spectra for the charge accumulation was performed using C1*s* peak ($E_B=284.6$ eV). According to Fig. 4a–c C1*s* spectrum for SiCN was deconvoluted into three components due to C–Si at 283.4 eV, C–C or C–H at 284.6 eV, C–O at 286.64 eV and O–C=O at 288.1 eV chemical bonds [12,24], respectively. Si–C chemical bonds are dominating in S and SS, while C–C bonds are at relatively low levels. The main existence form of C for SSC is C–C which is consistent with the result of Raman spectra. Si (2*p*) spectrum was decomposed into two spectra as shown in Fig. 4d. According to peak fittings, peaks Si–N and Si–C appear at 102.37 and 101.43 eV, respectively. It is clear that the obtained product is mainly constituted by Si–N and Si–C bonds. It is noted that no Si–O bonds, which should appear at 103 eV, are observed. Therefore, O (1*s*) originated from the absorbed gases, such as CO, CO_2, and H_2O. Consequently, C–C bonds appeared in the SiCN–Si_3N_4 ceramics of S and SS, but its content is quite low. SSC may be an ideal material in which free carbon dispersed uniformly in the amorphous SiCN with low conductivity.

The relative complex permittivity ($\varepsilon=\varepsilon'-j\varepsilon''$) is the key parameter for the characterization of dielectric properties of materials. According to the Debye theory, the real part (ε') of relative complex permittivity is related to the polarization relaxation, while the imaginary part (ε'') represents the dielectric loss of the materials [21]. The dielectric loss predicts the EMW absorbing capability of material, which can be used as a candidate of EMW absorber when its dielectric loss is high enough. The complex permittivity of Si_3N_4 and SiCN–Si_3N_4 ceramic as a function of frequency are shown in Fig. 5. The Si_3N_4 substrate is an insulator, whose ε' and ε'' are respectively 3.82 and 0.05 in X band frequency, so the complex permittivity of the SiCN–Si_3N_4 ceramic is determined mostly by the deposited SiCN. As shown in Fig. 4, the mean real part (ε'), imaginary part (ε'') of permittivity and dielectric loss ($\tan\delta$) of Si_3N_4 ceramic were 3.82, 0.05 and 0.014, respectively, which increased to 7.71, 6.94 and 0.899 after CVD/CVI of SiCN respectively. Compared with recent work on polymer-derived SiCN ceramics, LPCVI SiCN has relative low dielectric constant and higher dielectric loss which means good EMW absorbing properties. Known from the above

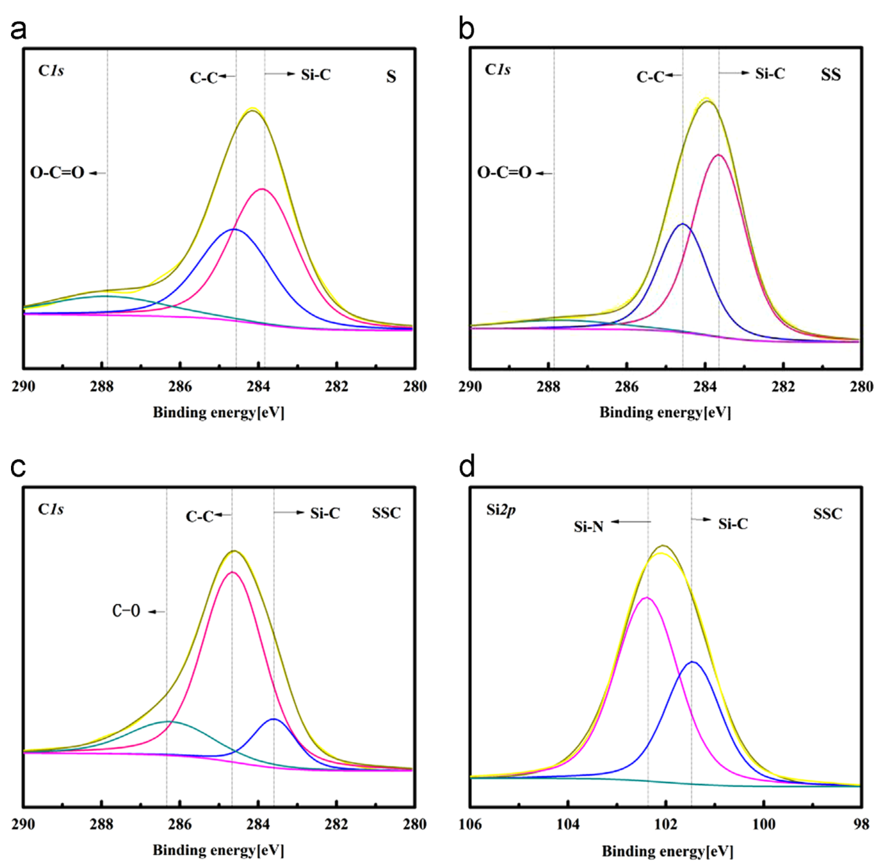

Fig. 4. High resolution XPS spectra of C1*s* levels for (a) S, (b) SS, (c) SSC and (d) Si2*p* core levels for SSC.

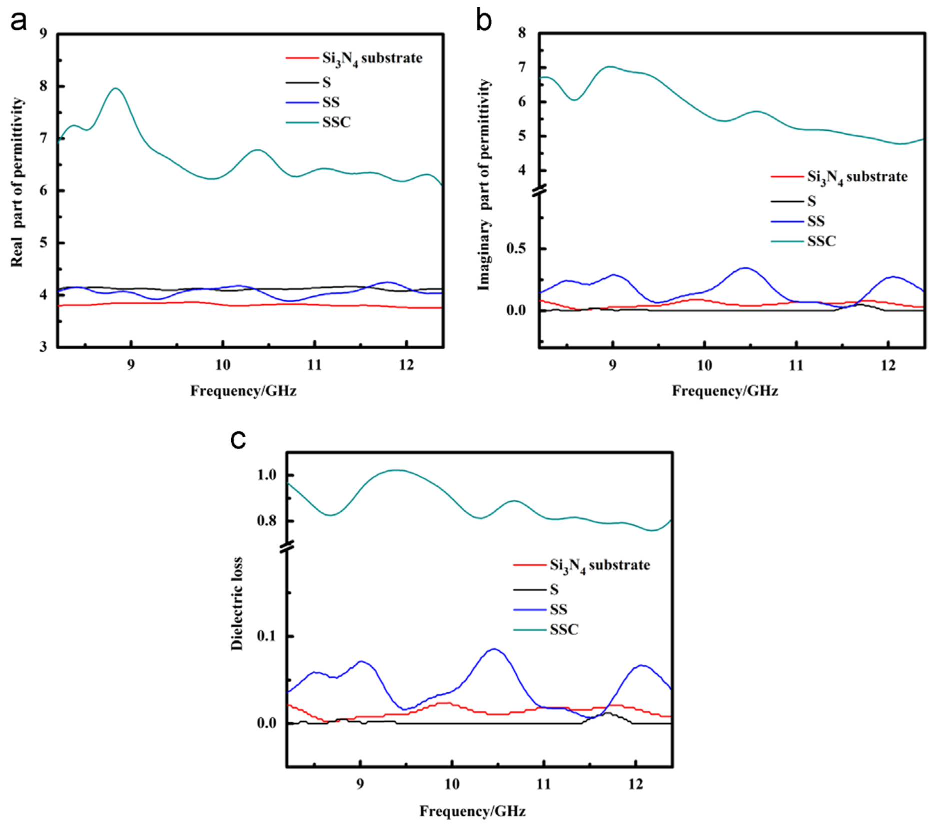

Fig. 5. (a) Real part (b) imaginary part of permittivity and (c) the dielectric loss (tan δ) as a function of frequency for Si_3N_4 and SiCN–Si_3N_4 ceramics.

results, the influence of Si_3N_4 substrate on the complex permittivity of the composite ceramics is ignored.

The real part (ε'), imaginary part (ε'') of permittivity and dielectric loss (tan δ) increased with increasing flux of C_3H_6, while the flux of $SiCl_4$ had little effect on that, which was attributed to the special carbon-rich structure of SiCN ceramics. First, most of the free electrons carried by the free carbon are separated by the amorphous phase. The electrons movement cannot happen in large scope, resulting in electronic relaxation polarization. The relaxation polarization takes long relaxation time and attenuates much EMW energy. Second, the interface charge polarization between free carbon and amorphous phase also needs to take a long relaxation time and can reduce EMW energy effectively, which is also an important factor for SiCN–Si_3N_4 to absorb EMW. In other words, free carbon plays the crucial role to absorb EMW as absorbing material and the dielectric loss (tan δ) can be controlled by changing the ratio of C_3H_6.

Suitable deposition velocity and dielectric properties of SiCN can be obtained by changing the ratio of precursor gases. Lower dielectric constant leads to the impendence match and weaken the surface reflection of the electromagnetic wave (EMW) [25,26] which promotes the improvement of EMW absorbing properties. Therefore, the work in the next step will be focused on optimizing the deposition parameters, including the ratios of precursor gases, deposition temperature, deposition time, etc.

4. Conclusion

The morphologies of SiCN–Si_3N_4 ceramics fabricated by LPCVD/CVI are continuous and dense. The deposition product is amorphous and mainly consists of Si–N, C–C, Si–C bonds. SiCN–Si_3N_4 ceramics possess suitable dielectric properties. The mean real part (ε') and imaginary part (ε'') of permittivity increase from 3.82 and 0.05 to 7.71 and 6.94. The dielectric loss (tan δ) can be controlled from 0.014 to 0.899 by changing the flux ratio of C_3H_6, which can be attributed to the unique structure of free carbon with high conductivity dispersing uniformly in the amorphous SiCN with low conductivity.

Acknowledgments

The authors acknowledge the support of the Chinese National Foundation for Natural Sciences under Contracts (nos. 51002120, 51032006, 50972119 and 51332004).

References

[1] X.M. Li, L.T. Zhang, X.W. Yin, Z.J. Yu, Mechanical and dielectric properties of porous Si_3N_4–SiC (BN) ceramic, Journal of Alloys and Compounds 490 (2010) 40–43.

[2] M.S. Cao, W.L. Song, Z.L. Hou, B. Wen, J. Yuan, The effects of temperature and frequency on the dielectric properties, electromagnetic interference shielding and microwave-absorption of short carbon fiber/ silica composites, Carbon 48 (2010) 788–796.

[3] B. Zhang, J.B. Li, J.J. Sun, S.X. Zhang, H.Z. Zhai, Z.W. Du, Nanometer silicon carbide powder synthesis and its dielectric behavior in the GHz range, Journal of the European Ceramic Society 22 (2002) 93–99.

[4] K.B. Sundaram, J. Alizadeh, Deposition and optical studies of silicon carbide nitride thin films, Thin Solid Films 370 (2000) 151–154.

[5] P. Bohacek, J. Huran, A.P. Kobzev, N.I. Balalykin, J. Pezoltd, PECVD silicon carbon nitride thin films: properties, in: Proceedings of the Seventh International Conference on Advanced Semi-conductor Devices and Microsystems, (2008) p. 191.

[6] W.J. Cheng, J.C. Jiang, Y. Zhang, H.S. Zhu, D.Z. Shen, Effect of the deposition conditions on the morphology and bonding structure of SiCN films, Materials Chemistry and Physics 85 (2004) 370–376.

[7] G. Singh, S. Priya, M.R. Hossu, S.R. Shah, Sachit Grover, A.R. Koymen, R.L. Mahajan, Synthesis of polymer-derived ceramic Si(B)CN-Carbon nanotube composite by microwave-induced interfacial polarization, Materials Letters 63 (2009) 2435–2438.

[8] Q. Li, X.W. Yin, L.Y. Feng, Dielectric properties of SiCN–Si_3N_4 composite ceramics in X-band, Ceramics International 38 (2012) 6015–6020.

[9] Bhandavat, W. Kuhn, E. Mansfield, J. Lehman, G. Singh, Synthesis of polymer-derived ceramic Si(B)CN-carbon nanotube composite by microwave-induced interfacial polarization, ACS-Applied Materials and Interface 4 (2012) 11–16.

[10] A. Izumi, K. Oda, Deposition of SiCN films using organic liquid materials by HWCVD method, Thin Solid Films 501 (2006) 195–197.

[11] T. Nakayamada, K. Matsuo, Y. Hayashi, A. Izumi, Y. Kadotani, Evaluation of corrosion resistance of SiCN films deposited by HWCVD using organic liquid materials, Thin Solid Films 516 (2008) 656–658.

[12] P. Jedrzejowski, J. Cizek, A. Amassian, J.E. Klemberg-Sapieha, J. Vlcek, L. Martinu, Mechanical and optical properties of hard SiCN coatings prepared by PECVD, Thin Solid Films 447–448 (2004) 201–207.

[13] L.F. Cheng, Y.D. Xu, L.T. Zhang, X.G. Luan, Oxidation and defect control of CVD SiC coating on three-dimensional C/SiC composites, Carbon 40 (2002) 2229–2234.

[14] Y.S. Liu, L.F. Cheng, L.T. Zhang, Y.H. Hua, W.B. Yang, Microstructure and properties of particle reinforced silicon carbide and silicon nitride ceramic matrix composites prepared by chemical vapor infiltration, Materials Science and Engineering A475 (2008) 217–223.

[15] X.W. Yin, Y.Y. Xue, L.T. Zhang, L.F. Cheng, Dielectric, electromagnetic absorption and interference shielding properties of porous yttria-stabilized zirconia/silicon carbide composites, Ceramics International 38 (2012) 2421–2427.

[16] X.F. Liu, L.T. Zhang, Y.S. Liu, F. Ye, X.W. Yin, Thermodynamic calculations on the chemical vapor deposition of SiCN from the $SiCl_4$-NH_3-C_3H_6-H_2-Ar system, Ceramics International 39 (2013) 3971–3977.

[17] X.W. Yin, X.M. Li, L.T. Zhang, L.F. Cheng, Y.S. Liu, T.H. Pan, Microstructure and mechanical properties of Lu_2O_3-doped porous silicon nitride ceramics using phenolic resin as pore-forming agent, International Journal of Applied Ceramic Technology 7 (2010) 391–399.

[18] T. Jiang, Y.S. Wang, Y.G. Wang, N. Orlovskaya, L.N. An, Quantitative Raman analysis of free carbons in polymer-derived ceramics, Journal of the American Ceramic Society 92 (2009) 2455–2458.

[19] S. Prawer, K.W. Nugent, Y. Lifshitz, G.D. Lempert, E. Grossman, J. Kulik, I. Avigal, R. Kalish, Systematic variation of the Raman spectra of DLC films as a function of sp^2:sp^3 composition, Diamond and Related Materials 5 (1996) 433–438.

[20] F. Tuinstra, J. Koenig, Raman spectrum of graphite, Journal of Chemical Physics 53 (1970) 126–1130.

[21] Q. Li, X.W. Yin, W.Y. Duan, L. Kong, B.L. Hao, F. Ye, Electrical, dielectric and microwave-absorption properties of polymer derived SiC ceramics in X band, Journal of Alloys and Compounds 656 (2013) 66–72.

[22] A.C. Ferrari, J. Robertson, Interpretation of Raman spectra of disordered and amorphous carbon, Physical Review B 61 (2000) 14095.

[23] K.W. Wang, B.S. Ma, Y.G. Wang, L.N. An, Complex impedance spectra of polymer-derived silicon oxycarbides, Journal of the American Ceramic Society 96 (2013) 1363–1365.

[24] O. Baghriche, S. Rtimi, C. Pulgarin, R. Sanjines, J. Kiwi, Effect of the spectral properties of TiO_2, Cu, TiO_2/Cu sputtered films on the bacterial inactivation under low intensity actinic light, Journal of Photochemistry and Photobiology A251 (2012) 50–56.

[25] C. Wang, X.J. Han, P. Xu, X.L. Zhang, Y.C. Du, S.R. Hu, et al., The electromagnetic property of chemically reduced graphene oxide and its application as microwave absorbing material, Applied Physics Letters 98 (2011) 072906–072908.

[26] R.C. Che, L.M. Peng, X.F. Duan, Q. Chen, X.L. Liang, Microwave absorption enhancement and complex permittivity and permeability of Fe encapsulated within carbon nanotubes, Advanced Materials 16 (2004) 401–405.